Electronic Supplementary Information

Hybrid Mn_3O_4–NiO nanocomposites as efficient photoelectrocatalysts towards water splitting under neutral pH condition

Hasimur Rahaman, Koushik Barman, Sk Jasimuddin* and Sujit Kumar Ghosh*

Department of Chemistry, Assam University, Silchar-788011, India

E-mail: sk.jasimuddin@aus.ac.in, sujit.kumar.ghosh@aus.ac.in

ESI 1. Absorption spectra of Mn_3O_4 nanoparticles and Mn_3O_4–NiO nanocomposites

The absorption spectral features and determination of the band gap of Mn_3O_4 nanoparticles and Mn_3O_4–NiO nanocomposites are shown in Fig. SI 1. Panel a shows the absorption spectra of Mn_3O_4 NPs and Mn_3O_4–NiO NCs measured in the solid state. The color change of Mn_3O_4–NiO nanocomposites is clearly seen before and after Mn_3O_4 conjugation. The original color of Mn_3O_4 particles is yellowish brown and that of NiO is greenish white, while the resulting Mn_3O_4–NiO nanocomposites are whitish brown. This suggests that the finally formed Mn_3O_4–NiO nanocomposites have inherited the colorimetric character of Mn_3O_4 nanoparticles. The electronic absorption spectrum of Mn_3O_4 shows three well-defined regions: the first portion from 250 to 310 nm, the second from 310 to 500 nm (with a maximum at 325 nm), and the third one finishing at 800 nm. The first portion is assigned to the allowed $O^{2-} \rightarrow Mn^{2+}$ and $O^{2-} \rightarrow Mn^{3+}$ charge-transfer transitions, and the last two can be reasonably related to d-d crystal-field transitions, $^3E_g(G) \leftarrow {}^3T_{1g}$, $^3A_{2g}(F) \leftarrow {}^3T_{1g}$, $^3A_{2g}(G) \leftarrow {}^3T_{1g}$, $^3T_{2g}(H) \leftarrow {}^3T_{1g}$, $^3T_{1g}(H) \leftarrow {}^3T_{1g}$, and $^3E_g(H) \leftarrow {}^3T_{1g}$, on octahedral Mn^{3+} species (S. Hirai, Y. Goto, Y. Sakai, A. Wakatsuki, Y. Kamihara and M. Matoba, *J. Phys. Soc. Jpn*. 2015 **84**, 114702, 1–6). Upon addition of nickel precursor and subsequent hydrolysis, the absorption spectrum of Mn_3O_4 becomes perturbed indicating electronic interaction between the components in maneuvering the nanocomposites (Y. M. Lee, C. −H. Hsu and H. −W. Chen, *Appl. Surf. Sci.*, 2009, **255**, 4658-4663). In addition, the appearance of a hump at around 325 nm could be ascribed to the band gap transition of NiO species in the composites (Y. M. Lee, C. −H. Hsu and H. −W. Chen, *Appl. Surf. Sci.*, 2009, **255**, 4658-4663). The direct band gap energy (E_g) of the Mn_3O_4 NPs and Mn_3O_4–NiO NCs could be determined by fitting the absorption data to the direct band gap transition equation as (S. Tsunekawa, T. Fukuda and A. Kasuya, *J. Appl. Phys.,* 2000, **87**, 1318–1321),

$$(\alpha h\nu)^2 = A(h\nu - E_g) \quad (1)$$

where, α is the absorption co-efficient, $h\nu$ the photon energy and A a constant. The absorption coefficient (α) is defined as: $\alpha = 2.303\ A/L\ c$, where, A is the absorbance of the sample, c the loading of sample (g L^{-1}), L the path length (= 1 cm). From the profiles (panel b) showing the plot of $(\alpha h\nu)^2$ as a function of $h\nu$, the estimated direct band gap of the Mn_3O_4 NPs and Mn_3O_4–NiO NCs is *ca.* 1.82 and 2.78 eV, respectively; these results show that the band gap of Mn_3O_4–NiO NCs is in-between free Mn_3O_4 and bulk NiO (4.0 eV) (R. J. O. Mossanek, G. Domínguez-Cañizares, A. Gutiérrez, M. Abbate, D. Díaz-Fernández and L Soriano, *J. Phys. Condens. Matter* 2013, **25**, 495506 1−7). The reduction in the band gap authenticates the interaction between the individual species in the composites.

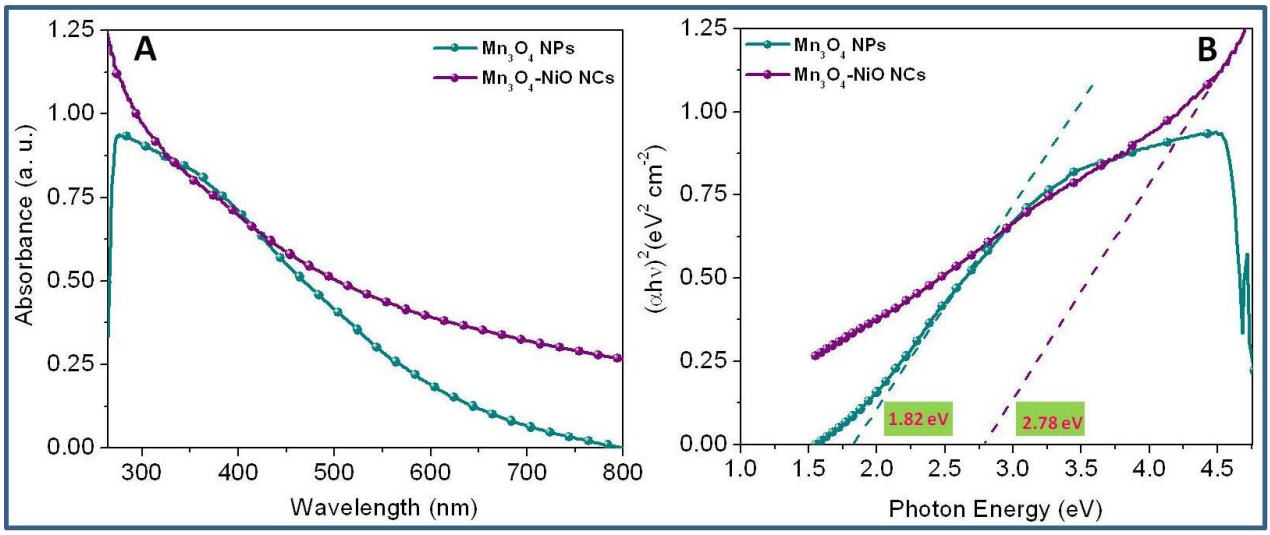

Fig. SI 1. (A) Solid state absorption spectra and (B) plot of $(\alpha h\nu)^2$ as a function of $h\nu$ of Mn_3O_4 NPs and Mn_3O_4–NiO NCs.

ESI 2. Fourier transform infrared spectra of Mn_3O_4 nanoparticles and Mn_3O_4–NiO nanocomposites

Fourier transform infrared spectra of Mn_3O_4 NPs and Mn_3O_4–NiO NCs are shown in Fig. SI 2. The FTIR spectrum of Mn_3O_4 (trace a) shows a lower region band at 451 cm^{-1}, that can be assigned to the Mn–O stretching vibrations (J. Tauc, R. Grigorvici and Y. Yanca, *Physica Status Solidi,* 1966, **15**, 627–637). The appearance of an additional band at 867 cm^{-1} is related to the stretching vibration of Mn–O–Mn species (R. J. O. Mossanek, G. Domínguez-Cañizares, A.

Gutiérrez, M. Abbate, D. Díaz-Fernández and L Soriano, *J. Phys. Condens. Matter*, 2013, **25**, 495506 1−7). Upon conjugation with the nickel oxide species (trace b), a doublet of peaks at 440 and 490 cm^{-1} could be assigned to Mn–O and Ni–O stretching vibrations, respectively (H. Guan, C. Shao, S. Wen, B. Chen, J. Gong and X. Yang, *Inorg. Chem. Commun*., 2003, **6**, 1302−1303) and the band for stretching vibration of Mn–O–Mn species moves to 880 cm^{-1} (D. L. S. Rodney, S. Mathieu, R. D. Prévot, Z. Z. Fagan, A. S. Pavel, M. K. J. Siu, T. Simon and P. B. Curtis, *J. Am. Chem. Soc.,* 2013, **135**, 11580−11586), which confirms the formation of Mn_3O_4–NiO NCs. Moreover, the presence of bands at 1406 and 1938 cm^{-1} could be attributed to the asymmetric and symmetric COO^- stretching vibrations of acetate chemisorption, respectively, which, probably, accounts for colloid stabilization (R. W. Johnston and D. C. Cronemeyer, *Phys. Rev. B*, 1954, **93**, 634−635). The broad band at 3180 cm^{-1} arises due to the stretching mode of O–H groups that reveals the existence of a small amount of water chemisorbed and/or physisorbed by the nanocomposites (K. Ito and H. J. Bernstein, *Can. J. Chem.*, 1956, **34**, 170–178).

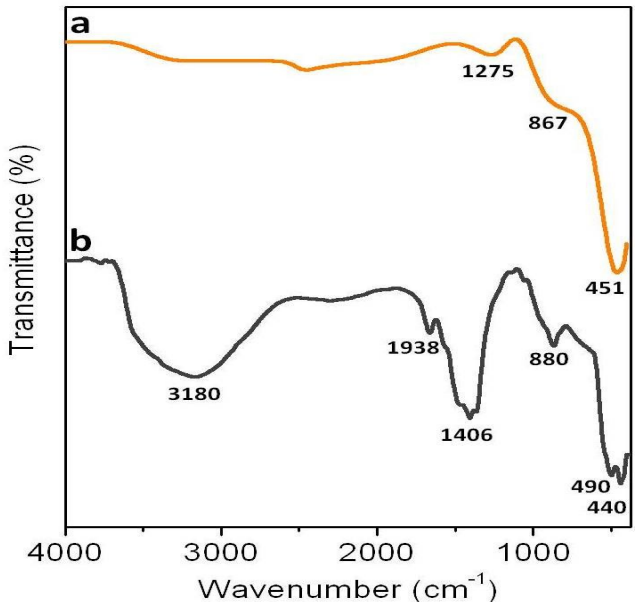

Fig. SI 2. Fourier transform infrared spectra of the (a) Mn_3O_4 NPs and (b) Mn_3O_4–NiO NCs.

ESI 3. Thermogravimetric analysis of Mn_3O_4–NiO nanocomposites

Thermogravimetric analysis (Fig. SI 3) of the as-dried powder sample shows two weight loss steps in the curve: 2.0 wt% loss corresponding to the water desorption (up to 200 °C), and a

weight loss of 4.5 wt % over 200–800 ºC as a result of the decomposition of the PVP polymer, verifying that the polymer molecules are, indeed, incorporated into the nanocomposites (H.-P. Cong and S.-H. Yu, *Adv. Funct. Mater*. 2007, **17**, 1814–1820).

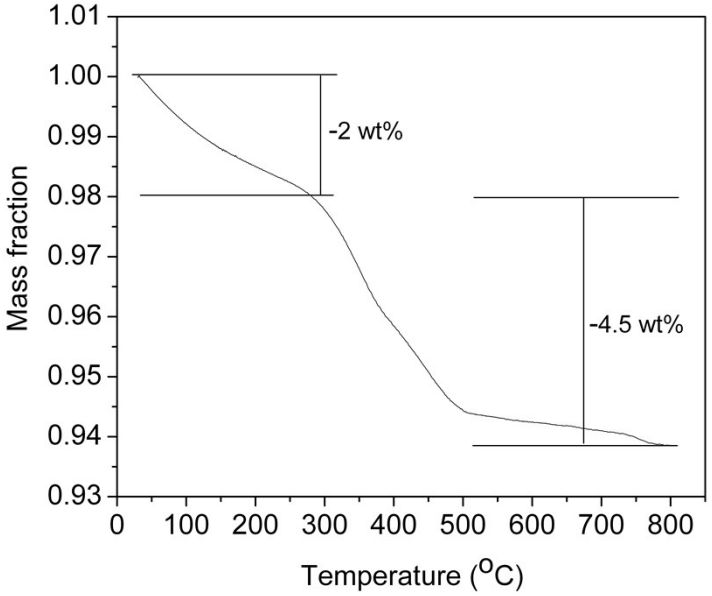

Fig. SI 3. TGA weight loss pattern of the as-synthesized Mn_3O_4–NiO NCs.

ESI 4. Electrode modification and characterisation

A mechanically and electrochemically cleaned gold electrode (2 mm in diameter) was immersed into an undisturbed colloidal dispersion of PVP-stabilised Mn_3O_4–NiO nanocomposites. After 6 h, a Mn_3O_4–NiO layer was formed over the gold electrode. The modified working electrode Mn_3O_4–NiO–Au was washed thoroughly with double distilled water and dried in nitrogen atmosphere for further use.

The modification of the gold electrode with the NCs (Fig. SI 4) has been confirmed by cyclic voltammetry (CV) and electrochemical impedance spectroscopy (EIS) using the redox probe $[Fe(CN)_6]^{3-/4-}$ in 0.1 M PBS at pH~7.0. The cyclic voltammogram of 0.05 mM $[Fe(CN)_6]^{4-}$ exhibits an irreversible redox couple at bare electrode. After modification of the gold electrode with Mn_3O_4–NiO NCs, a quasireversible couple (ΔE = 70 mV) with large current height has been obtained which is indicative of the better electronic communication between the probe and gold electrode through Mn_3O_4–NiO layer.

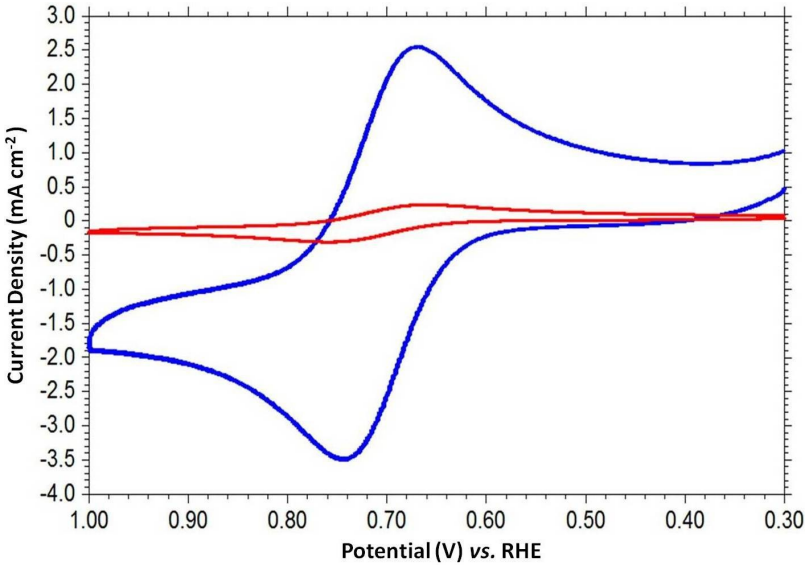

Fig. SI 4. Overlaid cyclic voltammogram of 0.5 mM $[Fe(CN)_6]^{4-}$ in 0.1 M PBS at pH~7.0 using bare (red) and Mn_3O_4–NiO modified (blue) gold electrode.

Electrochemical impedance spectroscopy of bare and Mn_3O_4–NiO modified gold electrode is shown in Fig. SI 5. The surface coverage (θ =0.92) has been obtained by using the equation, $\theta = [1-(i_p/i_p^o)]$, where, i_p (0.21 mA cm^{-2}) and i_p^o (2.58 mA cm^{-2}) are peak currents of the redox probe at bare and Mn_3O_4–NiO modified gold electrodes, respectively, under similar conditions. Therefore, electrochemical impedance spectroscopic analysis supports and supplements the observations through cyclic voltammetry.

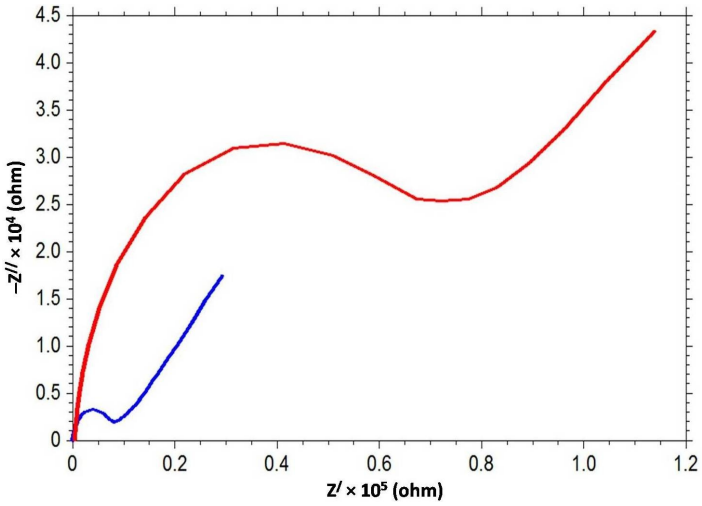

Fig. SI 5. Overlaid Nyquist plot ($-Z^{//}$ *versus* $Z^{/}$) of 0.5 mM $[Fe(CN)_6]^{4-}$ in 0.1 M PBS at pH~7.0 using bare (red) and Mn_3O_4–NiO modified (blue) gold electrodes.

ESI 5. Electrocatalytic oxidation of water at Mn_3O_4–NiO–Au electrode in acetate buffer solution

The electrocatalytic oxidation of water has also been tried in 0.1 M acetate buffer medium (pH ~ 7.0); interestingly, similar response has been observed in acetate buffer medium (Fig. SI 6). Moreover, it was also noted that no such oxidation peak could be observed at Mn_3O_4–NiO–Au electrode in non-aqueous media, like, acetonitrile (CH_3CN) or dichloromethane (CH_2Cl_2) etc. which indicates that the evolution of oxygen occurs from the oxidation of water. In addition, upon addition of water in acetonitrile solvent (containing 0.1 M $[Bu_4N][ClO_4]$, pH~7.0), an oxidative peak appears at ~ +1.5 V. These observations points out that the evolution of oxygen from water oxidation in the presence of nanocomposites are not restricted to the presence of phosphate buffer saline only; it can happen in buffer media with desired pH.

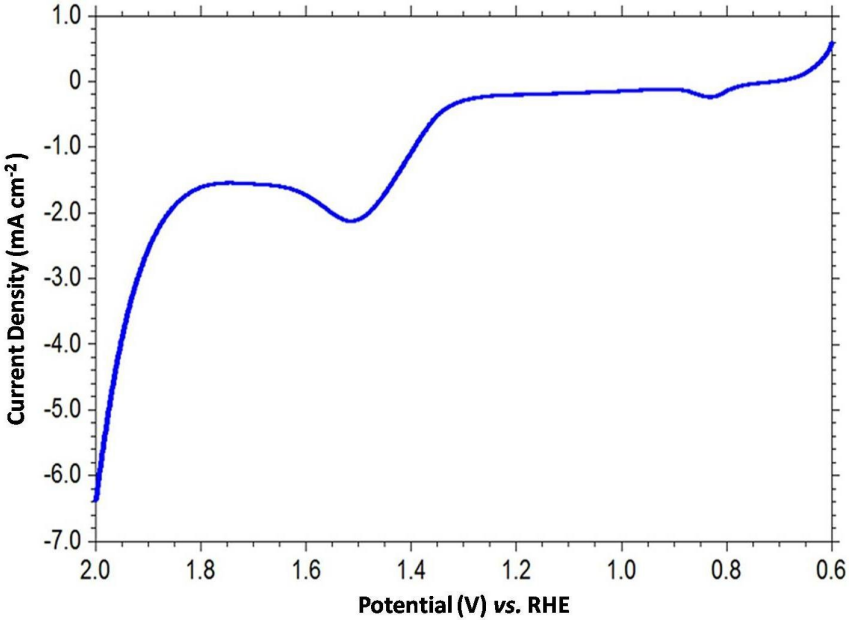

Fig. SI 6. Linear sweep voltammogram obtained at Mn_3O_4–NiO–Au electrode at 0.1 M acetate buffer solution (pH~7.0).

ESI 6. Electrocatalytic oxidation of water at Mn_3O_4–NiO–Au electrode with different scan rates

The linear sweep voltammogram (Fig. SI 7) for the oxidation of water obtained with Mn_3O_4–NiO–Au electrode at 0.1 M PBS (pH~7.0) has been measured at different scan rates. It is seen that the oxidation peak current increases with the scan rate in the range of 50–100 mV s^{-1} and follows the linear regression equation (as shown in the inset), J (mA cm^{-2}) = 0.0136 V + 1.0629 (R^2 = 0.9984), which confirms that the electro-oxidation of water at the Mn_3O_4–NiO modified electrode is a surface-controlled process (M. Zhang, M. de Respinis and H. Frei, *Nature Chem*., 2014, **64**, 362–367).

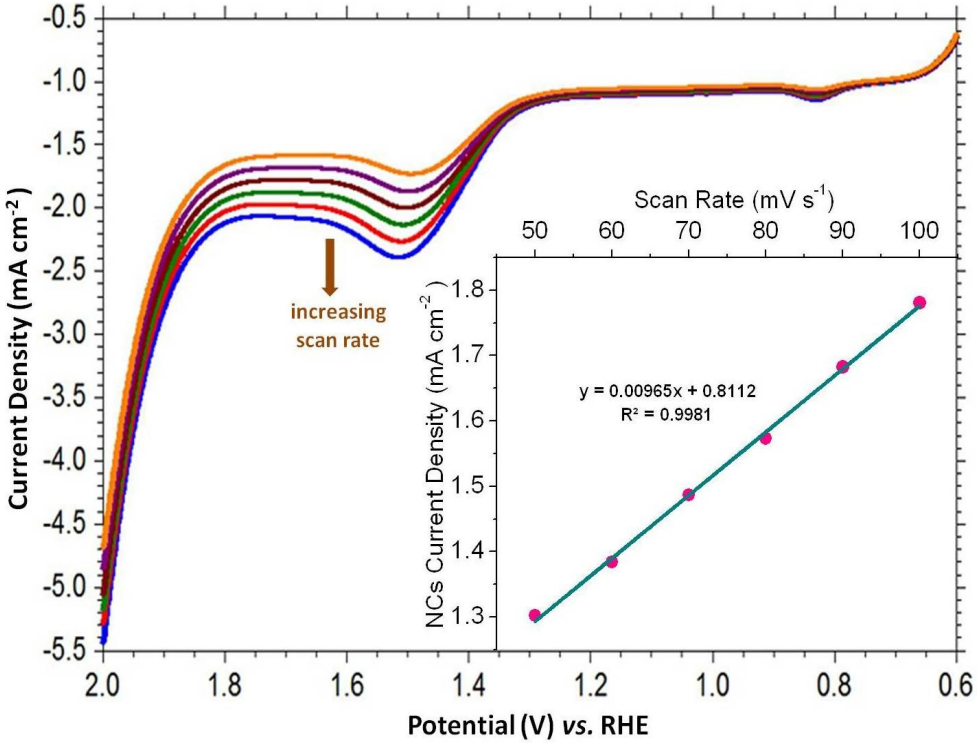

Fig. SI 7. Linear sweep voltammogram obtained with Mn_3O_4–NiO–Au electrode in 0.1 M PBS (pH~7.0) at different scan rates. A plot of current density of the nanocomposites as a function of scan rate is shown in the inset.

ESI 7. Cyclic voltammogram of 0.1 M PBS (pH~7.0) at Mn_3O_4–NiO–Au electrode

Fig. SI 8 presents the cyclic voltammogram of 0.1 M PBS (pH~7.0) at Mn_3O_4–NiO–Au electrode.

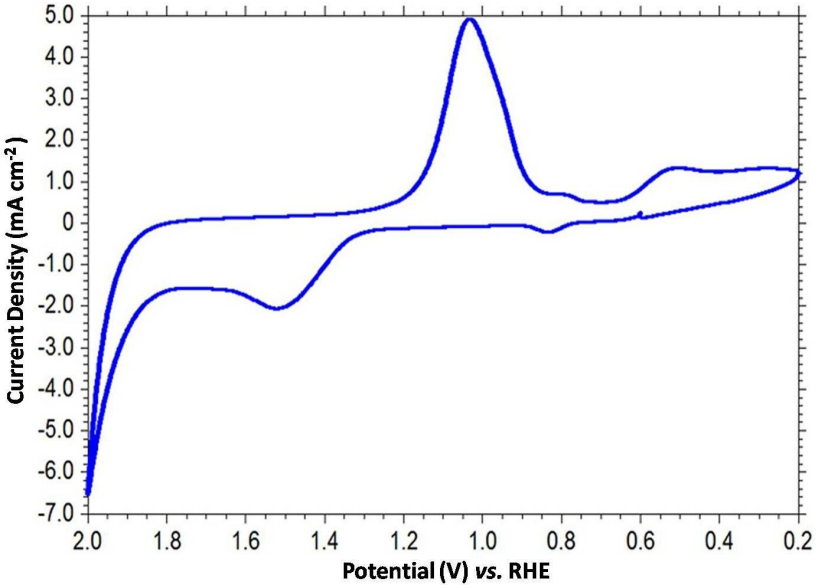

Fig. SI 8. Cyclic voltammogram of 0.1 M PBS (pH~7.0) at Mn_3O_4–NiO–Au electrode.

ESI 8. Electrocatalytic oxidation of water at Mn_3O_4–NiO–Au electrode at different pH

The effect of pH on the electrocatalytic oxidation of water at Mn_3O_4–NiO–Au electrode has been studied in the pH range of 5.0 – 9.0. Fig. SI 9 illustrates the linear sweep voltammogram at varying pH values of PBS at Mn_3O_4–NiO–Au electrode. It is seen that the anodic peak potential is shifted towards the more negative potential with increasing pH of the medium. The oxidation peak potential varies linearly with increasing pH and follows the linear regression equation, E_{pa} = -0.059 pH + 1.927, R^2 = 0.9968 (as shown in the inset). The slope of 59 mV per pH unit indicates that equal number of protons and electrons are involved in the electrode reaction process (G. Dryhurst, *Electrochemistry of Biological Molecules*. 1977, **2**, 16-17).

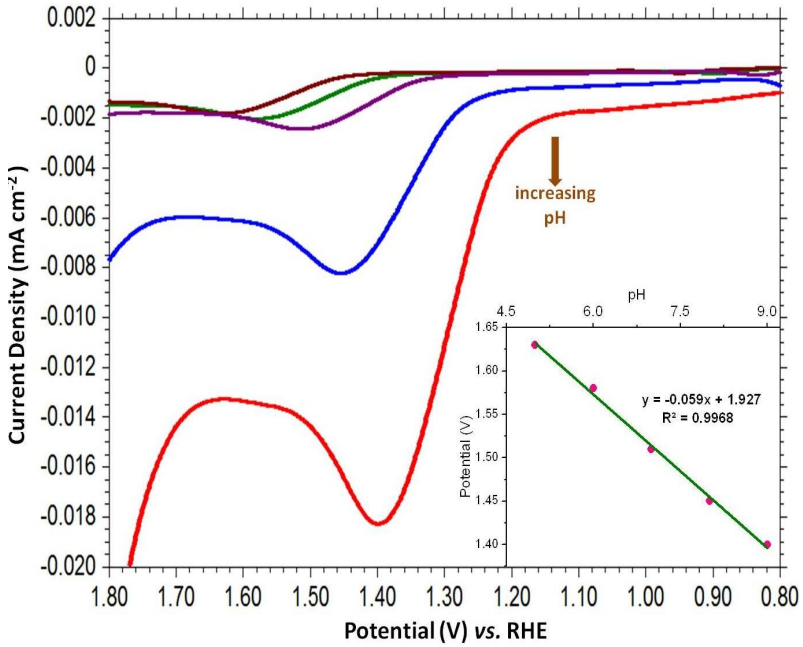

Fig. SI 9. Overlaid linear sweep voltammogram derived from Mn_3O_4–NiO–Au electrode at different pH of 0.1 M PBS (5.0, brown; 6.0 green; 7.0, violet, 8.0, blue and 9.0, red) at a scan rate of 100 mV s^{-1}. Inset shows the plot of oxidation peak potential as a function of pH.

ESI 9. Chronopotentiogram during electrocatalytic oxidation of water with Mn_3O_4–NiO modified electrode under neutral pH condition

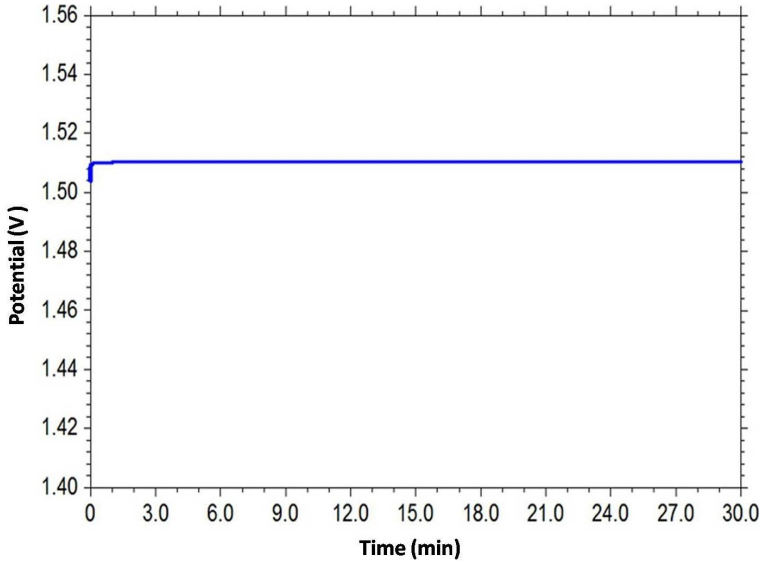

Fig. SI 10. Chronopotentiogram with Mn_3O_4–NiO modified electrode in 0.1 M PBS (pH~7.0) at 2.5 mA cm^{-2}.

Chrono-potentiometry (Fig. SI 10) at Mn_3O_4–NiO–Au electrode in 0.1 M PBS (for 30 min at 2.5 mA cm^{-2}) also supports the good stability of the electrode during electrolysis of water.

ESI 10. Oxygen evolution curve during electrocatalytic oxidation of water with Mn_3O_4–NiO modified electrode under neutral pH condition and digital camera photograph showing the bubbling of oxygen on the electrode surface

A digital photograph showing the evolution of gas bubbles and oxygen evolution curve during the electrocatalytic oxidation of water on Mn_3O_4–NiO modified electrode surface is shown in Fig. SI 11.

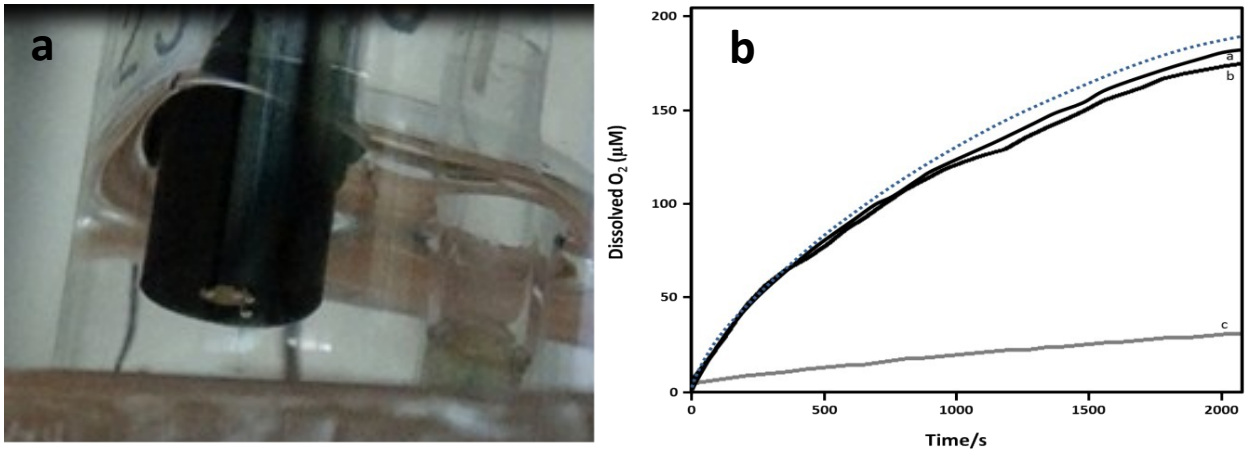

Fig. SI 11. (a) Digital photograph showing the bubbling of oxygen on the electrode surface, (b) Oxygen evolution during the controlled potential electrolysis of water in a gas-tight electrochemical cell containing 0.1 M PBS (pH~7.0) at bare Au (curve c) and Mn_3O_4–NiO–Au electrodes in the presence of sunlight (curve b) and ultraviolet light (curve a) as measured with a fluorescence probe. Dotted line represents the theoretical oxygen evolution with 100% efficiency.